

Exoskeletal strength and cuticle composite profile of the acorn weevil rostrum

M. Andrew Jansen,^{1,*} Jason Williams,² Nikhilesh Chawla,² and Nico M. Franz¹

¹School of Life Sciences, Arizona State University, Tempe, AZ 85287, USA

²School for Engineering of Matter, Energy, and Transport,
Arizona State University, Tempe, AZ 85287, USA

(Dated: March 28, 2019)

The acorn weevil (*Curculio* Linnaeus, 1758) rostrum (snout) exhibits remarkable flexibility and toughness derived from the microarchitecture of its exoskeleton. Here we characterize modifications to the composite profile of the rostral cuticle that simultaneously enhance the flexibility and fracture toughness of the distal portion of the snout. Using Classical Lamine Plate Theory, we estimate the effect of these modifications on the elastic behavior of the exoskeleton. We show that the tensile behavior of the rostrum across six *Curculio* species with high morphological variation correlates with changes in the relative layer thicknesses and orientation angles of layers in the exoskeleton. Accordingly, increased endocuticle thickness is strongly correlated with increased tensile strength. Rostrum stiffness is shown to be inversely correlated with fracture toughness; thus allowing a highly curved rostrum to completely straighten without structural damage. Finally, we identify exocuticle rich invaginations of the occipital sutures both as a likely site of crack initiation in tensile failure, and as a source of morphological constraint on the evolution of the rostrum in *Curculio* weevils.

The exoskeleton of Coleoptera (beetles) is a hierarchically structured, fibrous composite – characterized by variously arranged α -chitin (N-acetylglucosamine) nanofibrils that are embedded in a heterogeneous protein matrix [1–3]. Although α -chitin is brittle and strongly anisotropic, beetle cuticle is simultaneously rigid and tough due to its unique laminate microstructure (reviewed in [4–6]), characterized in detail below. Impact-prone areas and exaggerated structures in arthropods generally exhibit cuticle organization that resists deformation and fracture [7–11]. However, acorn weevils in the genus *Curculio* Linnaeus, 1758¹ (Curculionidae in the sense of [13]) instead exhibit unusual distal flexibility in an elongate extension of the head called the rostrum (snout) [1, 14–16]. The rostrum is a hollow, strongly curved (over 90° in some species), cylindrical, exoskeletal extension of the otherwise nearly-spherical head, which bears at its apex the terminal chewing mouthparts [16–20]. This structure is used by the female to feed on fruit (plant) tissue and to excavate sites for egg-laying (oviposition, see Fig. 1). The rostrum can be repeatedly bent, without evident damage, and despite being composed of the same material as other rigid body parts [1, 14–16]. By maintaining constant pressure on the snout and rotating around the bore-hole, females are able to flex the rostrum into a straightened configuration and produce a linear channel into the fruit. A single adult female may prepare hundreds of such sites [15, 21, 22].

Despite its documented performance in many *Curculio*

species [15, 16, 21, 22], it remains unknown how the rostrum of female acorn weevils can withstand the repeated, often extreme bending incurred during the process of egg-chamber excavation. In this study, we therefore characterize the composite profile of the rostral cuticle to account for the observed flexibility of the snout. We show that the relative layer thicknesses and fiber orientation angles of the exocuticle and endocuticle of the rostrum are strongly differentiated from the head capsule and other body parts. The effect of these differences on the elasticity of the cuticle is estimated using Classical Laminate Plate Theory (CLPT). Recent studies have shown that the yield strength of the beetle exoskeleton is lower in tension than compression [23]. To assess the validity of these findings, we compare the ultimate tensile strength of the rostrum across species and snout morphotypes. We also report displacement-controlled load cycling results for the snout of one *Curculio* species with strongly curved morphology. Our results indicate that an increase in the volume fraction of endocuticle in the rostrum conveys higher tensile strength at the rostral apex across all tested species; and further, that a strongly curved rostrum can be flexed repeatedly without harm to the structure.

We additionally describe the fracture mechanics of the snout, while considering how modification of the cuticle may prevent crack formation during oviposition. Accordingly, the flexibility and tensile strength of the rostrum appear to be derived exclusively from modification of the composite architecture of the exoskeleton. This is the first time that a modified composite profile has been reported as a means of enhancing structural elasticity in the insect exoskeleton (though see [24]).

* corresponding author, email: majanse1@asu.edu

¹Pursuant to the International Code of Zoological Nomenclature, the first mention of any specific epithet will include the full genus and species names as a binomen (two-part name) followed by the author and date of publication of the name. This is not an in-line reference; it is a part of the name itself and refers to a particular act establishing the validity and fixing the identity of the corresponding name by that author [12].

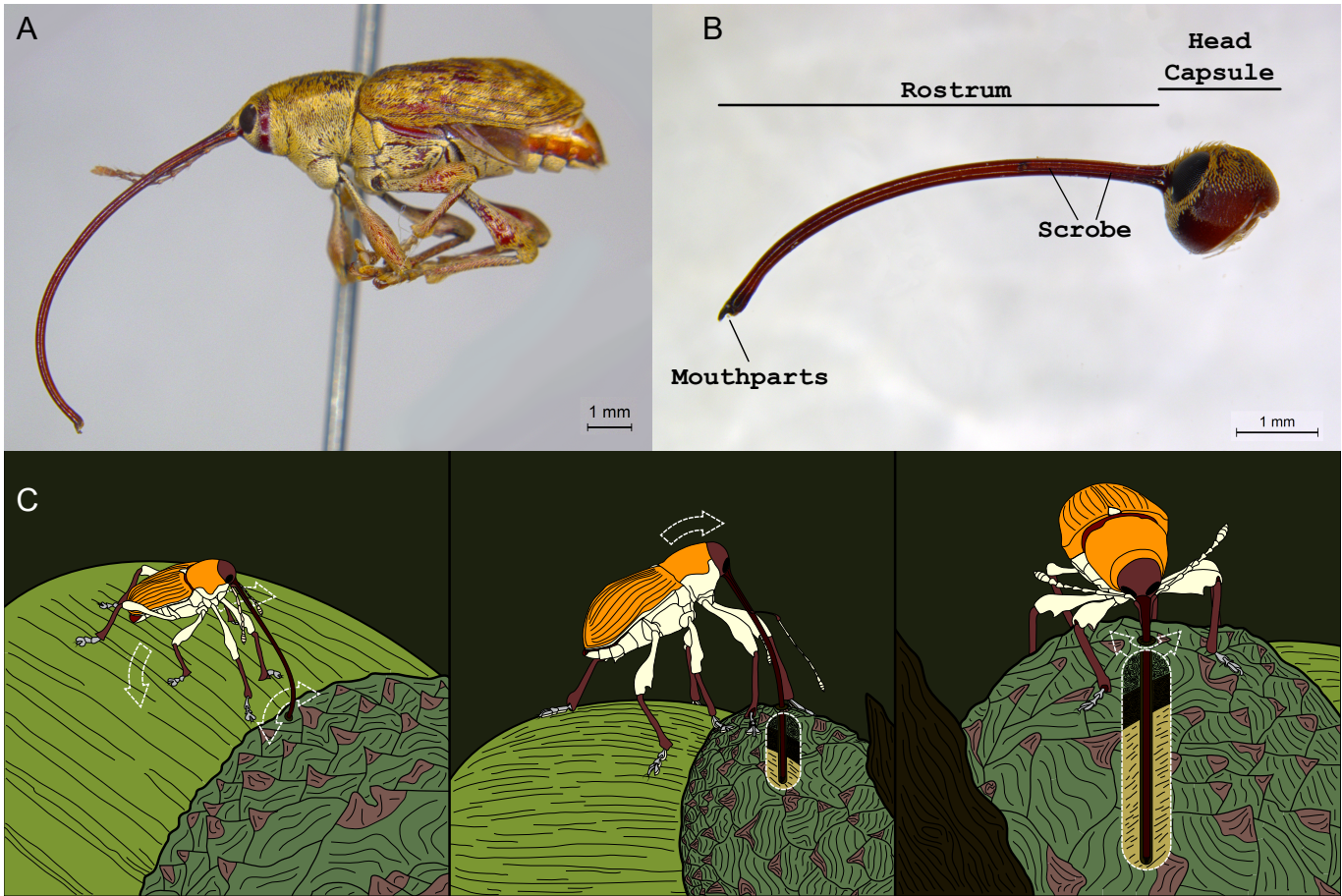


FIG. 1. Morphology and oviposition behavior of female *Curculio* weevils. **a**, Lateral habitus image of female *Curculio sayi* (Gyllenhal, 1836) featuring the elongate, strongly curved rostrum. **b**, Lateral view of head of female specimen of *Curculio longinasus* Chittenden, 1927, with major anatomical features indicated. **c**, Illustration of oviposition behavior, proceeding from left to right: female makes incision in host fruit, flexes head directly over bore-hole using front legs, then maintains tension on snout while rotating to excavate linear channel into fruit. During this process, female rostrum is bent until completely straight.

69 I. MICROSTRUCTURE OF THE CURCULIO 70 ROSTRUM

71 In arthropods – including beetles – the exocuticle is
72 comprised of numerous unidirectional laminae of chitin
73 nanofibrils. Each layer is the thickness of a single fiber
74 (2-4 nm) embedded in a proteinaceous matrix [25, 26].
75 These layers are stacked at a more or less constant an-
76 gle to each other, forming a quasi-isotropic laminate
77 known as the Bouligand structure [6, 27, 28]. This lay-
78 out effectively mitigates the strong anisotropy of α -chitin,
79 thus yielding a versatile building material for the ex-
80 oskeleton [2, 25, 26, 29]. Beetle endocuticle, however,
81 is unique among arthropods and is comprised of large
82 – 1-5 μm diameter in *Curculio* – unidirectional bun-
83 dles of chitin, called macrofibers. Chitin macrofibers
84 are orthotropic (axial: $E_1 = 8.5 \text{ GPa}$; transverse:
85 $E_2 = E_3 = 0.52 \text{ GPa}$ [1]), and arranged in uni-
86 directional plies, as depicted in Figs. 2, 3 [4, 5]. Typi-
87 cally, adjacent macrofiber laminae are paired and pseudo-

88 orthogonal – i.e., angled nearly 90° to each other (see
89 Fig. 3; [30]) – with a constant stacking angle between
90 pairs, although other configurations have been observed
91 [3–5, 31]. This geometric sequence of the macrofiber lam-
92 inae yields an approximately transversely isotropic com-
93 posite, similar to the Bouligand structure [5, 26]. No-
94 tably, the resulting laminate is less rigid than the exocu-
95 ticle, but exhibits greater toughness because the pseudo-
96 orthogonal plies effectively inhibit crack formation and
97 propagation between successive layers [3–5].

98 Serial thin sectioning and scanning electron microscopy
99 of fractured *Curculio* specimens reveals that endocuti-
100 cle in the head capsule fits this general profile, with an
101 angle of nearly 30° between successive pairs of pseudo-
102 orthogonal plies. Additionally, in the head capsule,
103 the thickness of the exocuticle and endocuticle in cross-
104 section is nearly equal – typically between 20-30 μm .
105 However, the cuticle composite lay-up of the rostral apex
106 is strongly differentiated from the head capsule, as shown
107 in Fig. 3. Distally the exocuticle is reduced to a thin shell

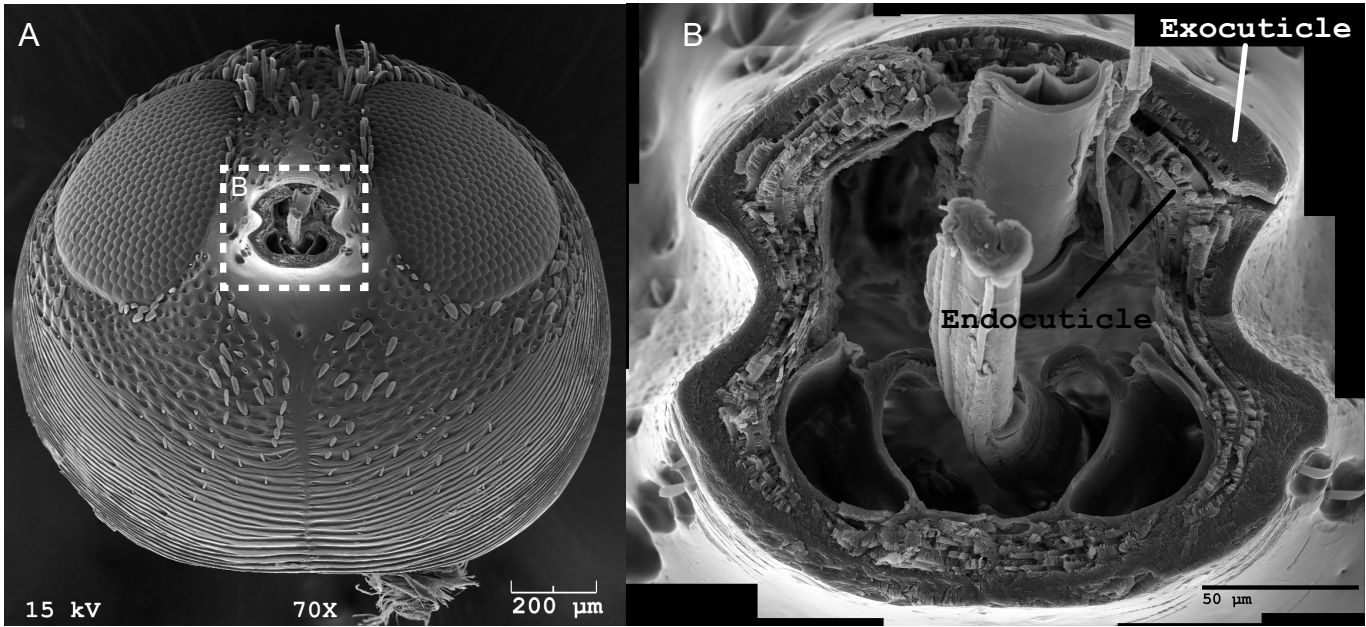


FIG. 2. Gross divisions of cuticle in the female *Curculio* rostrum. **a**, Scanning electron micrograph of head capsule, in frontal view, of female *Curculio sulcatulus* (Casey, 1897), with rostrum removed. **b**, Magnified view of junction between rostrum and head capsule, showing division of cuticle into two general regions: exocuticle and endocuticle.

(ca. 5 μm), with the endocuticle thickened to offset this reduction and maintain a constant cuticle thickness (ca. 50 μm total) throughout its length. Moreover, the endocuticular macrofibers exhibit no rotation between successive pseudo-orthogonal plies; and are oriented at approximately $\pm 45^\circ$ to the longitudinal axis of the snout (i.e., an antisymmetric [$\pm 45^\circ$] angle-ply laminate). We previously identified these modifications to the composite structure of the cuticle within a single species, *Curculio longinasus* Chittenden, 1927 [1, 14]. However, this composite profile is herein reported in the rostrum of six additional, phylogenetically disjoint, species, suggesting that this is an evolutionarily conserved trait throughout the genus *Curculio*. In all examined species, the portion of the snout between the head capsule and apex of the scrobe exhibits a gradual transition in composite profile along an anterior-posterior gradient.

Here we estimate the effect of differential cuticle organization on uni-axial membrane and on transverse flexural Young's moduli of the cuticle in the rostral apex and head capsule using CLPT [32, 33]. The effective elastic constants of the cuticle regions of *Curculio longinasus* – estimated previously [1] – are used to construct constitutive equations for the entire cuticle of that species.

The cuticle of the head capsule is estimated to have membrane and flexural moduli of $E_m = 4.77 \text{ GPa}$ and $E_f = 6.04 \text{ GPa}$, respectively. In the rostral apex these values are reduced by approximately 72% and 60%, respectively ($E_m = 1.36 \text{ GPa}$; $E_f = 2.44 \text{ GPa}$). Two hypothetical cuticle lay-ups are also modeled to individually assess the contributions of either modified layer thickness or stacking angle sequence to the cuticle's flexibility. The

effective moduli of a configuration with the angle stacking sequence of an otherwise typical cuticle (i.e., in the head capsule) that shows layer thicknesses of the rostral apex are calculated as $E_m = 3.73 \text{ GPa}$, $E_f = 4.31 \text{ GPa}$; representing 22% and 29% decreases from unmodified cuticle, respectively. Similarly, a hypothetical cuticle with the layer thicknesses of ordinary cuticle yet possessing the angle stacking sequence of the rostral apex (i.e., $\pm 45^\circ$ angle-ply in the endocuticle) has effective elastic moduli of $E_m = 3.77 \text{ GPa}$, $E_f = 5.76 \text{ GPa}$; representing 21% and 4.7% decreases from unmodified cuticle, respectively. Each of the cuticle modifications noted in the rostral apex individually decrease the elastic moduli of the cuticle. However, they appear to have a synergistic combined effect on cuticle elasticity, rather than a simple additive effect. This result suggests that both modifications are necessary in order for the snout to function properly in the living individual – where the combined effect allows the rostrum to bend until completely straight without fracture.

II. FORCE-CONTROLLED LOADING TO FRACTURE

To better characterize the failure behavior of the female rostrum, we performed tensile testing on the snouts of six *Curculio* species that representing a mixture of closely and distantly related taxa [34–37]. Each specimen was first immersed in di-H₂O for 24 hours to simulate the living tissue (see [38]), then subjected to force-controlled, uniaxial loading to fracture at a constant stress rate

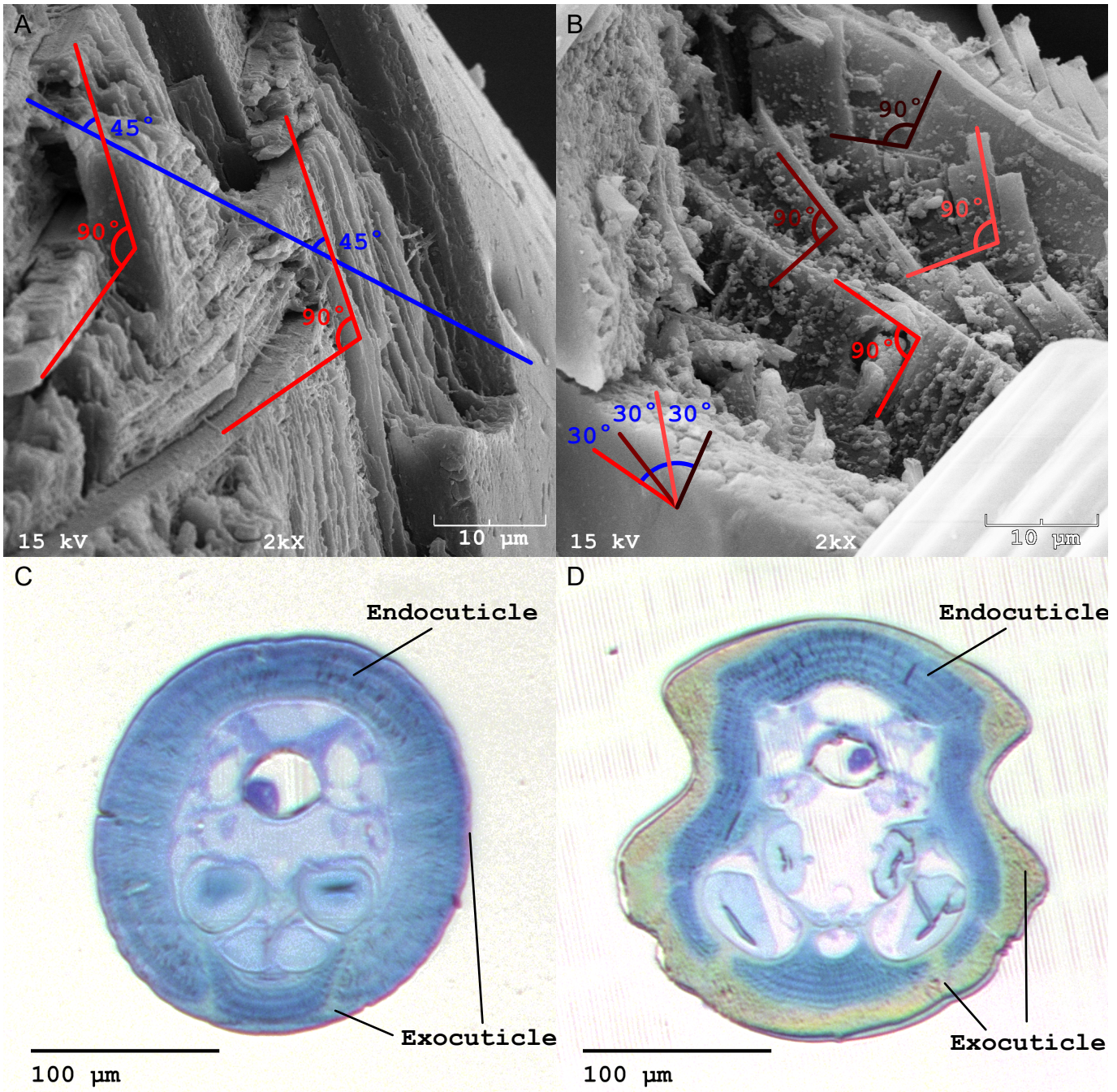


FIG. 3. Composite profiles of rostral *Curculio* cuticle. **a**, Scanning electron micrograph of fractured specimen of *Curculio humeralis* (Casey, 1897), showing that cuticle of rostral apex is organized as $\pm 45^\circ$ angle-ply laminate. **b**, Scanning electron micrograph of fractured specimen of *Curculio caryae* (Horn, 1873), showing that cuticle of rostral base and head capsule has approximately 30° stacking angle between each pair of pseudo-orthogonal plies. **c–d**, Semi-thin sections of cuticle from specimen of *Curculio humeralis*, stained with toluidine-blue-borax; demonstrating: (**c**) that exocuticle of rostral apex is reduced to thin shell close to $5\text{ }\mu\text{m}$ thick, with endocuticle thickened to maintain a constant laminate thickness; and, (**d**) that exocuticle of head capsule and base of snout occupies nearly half of through-thickness of cuticle.

of $1.0\text{ gf}\cdot\text{s}^{-1}$. In general, the specimens exhibited a non-linear viscoelastic response curve characterized by a sharp increase in stress at higher strains, terminating in brittle fracture [39]. We suggest that strain hardening occurs as the longitudinal axis of the macrofibers becomes more closely aligned to the cylindrical axis of the rostrum, thereby resisting tension more directly with increasing strain [40].

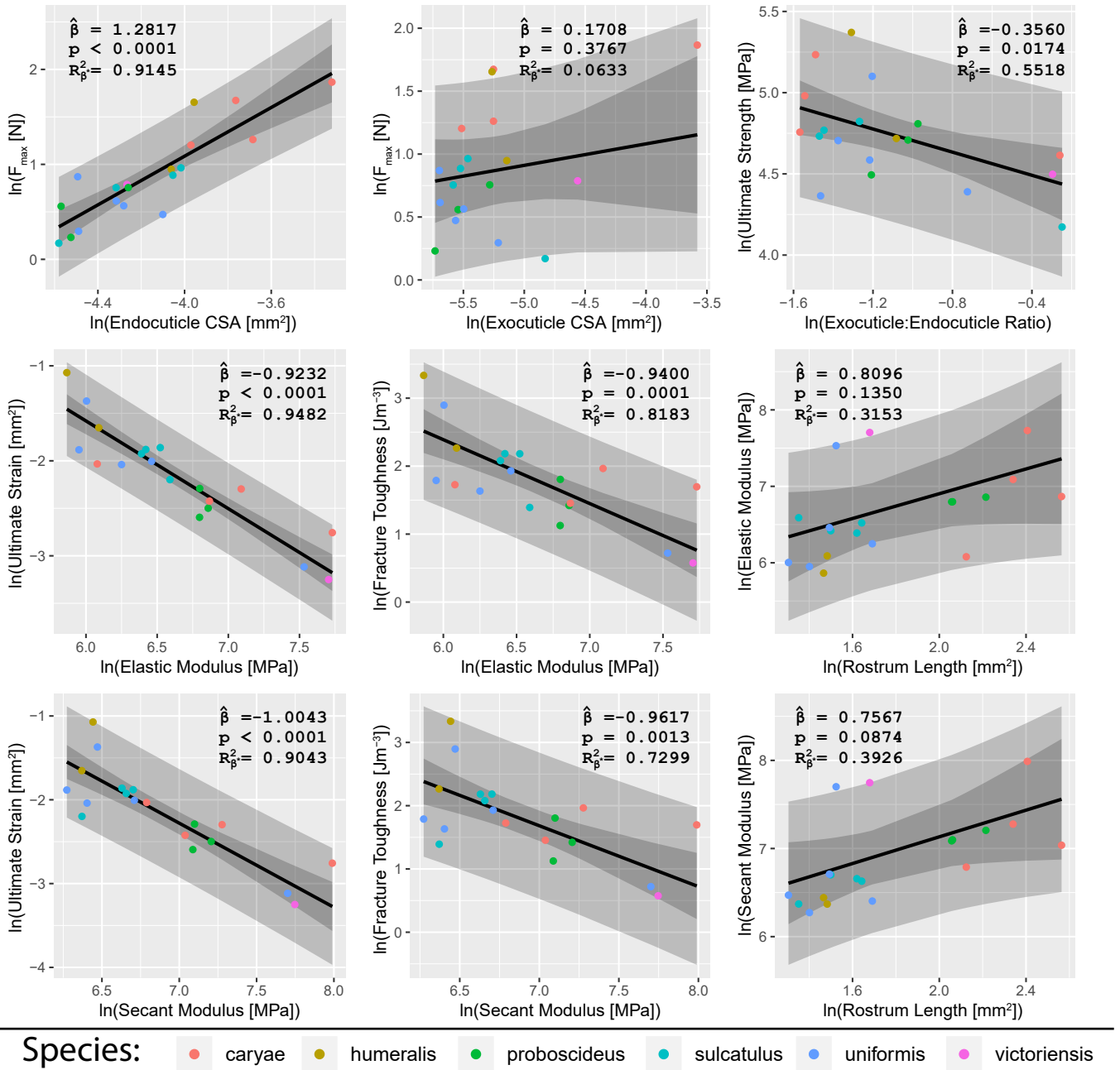


FIG. 4. Tensile properties of the female *Curculio rostrum*. Each plot shows relationship between two variables as predicted by phylogenetic linear mixed-effect model; with species as random effect and variance-covariance matrix generated from Brownian motion over preferred phylogeny of [35]. Gray regions represent the prediction interval and bootstrapped 95% confidence interval of model. The estimated fixed effect $\hat{\beta}$ is given, along with p-value of t-test assessing whether $\hat{\beta}$ is significantly different from zero. Generalized marginal $R^2_{\beta^*}$ for assessing fixed effects is also reported. In general, increased endocuticle thickness is associated with greater tensile strength, and stiffness is inversely correlated with toughness.

We also examined the correspondence between composite structure and mechanical behavior of the snout in an evolutionary, comparative context. Phylogenetic linear mixed effects models (PGLM, Fig. 4) were used to account for phylogenetic non-independence in residual variance, with species membership included as a random effect [41, 42]. The resulting models show that the max-

imum force sustained at the site of failure is strongly correlated with the cross-sectional area of the endocuticle ($\hat{\beta} = 1.28$, $p < 0.0001$), and not the exocuticle ($\hat{\beta} = 0.17$, $p = 0.38$), at that site. There is thus a negative correlation between ultimate tensile strength of the specimen and the cross-sectional exocuticle-to-endocuticle area ratio at the fracture site ($\hat{\beta} = -0.36$, $p = 0.017$).

191 Although CLPT predicts a positive association between
 192 the proportion of exocuticle and stiffness of a generalized
 193 cuticle, we found no evidence of correspondence between
 194 the cross-sectional properties of the fracture site and the
 195 overall performance of the rostrum. This result is not
 196 too surprising however; because the cross-sectional ar-
 197 eas of the cuticle regions vary across the length of the
 198 head along an anterior-posterior gradient, it is not possi-
 199 ble to correlate measurements from the fracture surface
 200 to properties of the entire rostrum.

201 Instead, we found that the uniaxial elastic modulus
 202 (low strain: E_{low}) and secant modulus at failure (E_{sec})
 203 were inversely correlated with ultimate strain and frac-
 204 ture toughness (see Fig. 4). This implies that stiffer
 205 specimens – and by extension, stiffer cuticle profiles –
 206 are generally more brittle. We also observed a moder-
 207 ate, but not statistically significant, stiffening size-effect
 208 with respect to rostral length. This runs contrary to
 209 our expectation that a longer, more strongly curved ro-
 210 strum would require increased flexibility to avoid fracture
 211 during oviposition [36, 37]. It is possible that longer ro-
 212 stra also have a longer transition gradient from basal to
 213 apical profile; thereby reinforcing the junction between
 214 the rostrum and head capsule against buckling. Young’s
 215 modulus of the rostrum would be comparatively higher
 216 in such species, due to the higher volume fraction of ex-
 217 ocuticle. We therefore posit that the gross elastic per-
 218 formance of the cuticle is consistent across the weevil
 219 genus *Curculio*. A single mechanism – i.e., the modi-
 220 fied composite profile – likely confers increased flexibility
 221 and tensile strength to the rostral apex across all *Cur-*
222 culio species. In addition, the endocuticle demonstra-
 223 bly contributes more to rostral tensile strength than the
 224 exocuticle; likely because of its organization into large
 225 bundles of aligned, anisotropic fibers, and amounting a
 226 trade-off between rigidity and toughness. Consequently,
 227 the altered composite profile of the cuticle in the rostral
 228 apex makes the rostrum simultaneously more flexible and
 229 fracture-resistant.

230 III. LOAD CYCLING OF THE PECAN WEEVIL

231 To confirm that repeated, prescribed straightening of
 232 the rostrum does not result in damage to the cuticle,
 233 we performed displacement-controlled fatigue testing on
 234 a typical female specimen of the pecan weevil *Curculio*
235 carya (Horn, 1873) – a species that exhibits extreme
 236 (80–90°, Fig. 5) rostral curvature [16, 21]. The specimen
 237 was aligned so that uniaxial tension would induce elon-
 238 gation of the distal portion of the rostrum with minimal
 239 off-axis deflection of the uncurved section. The strain
 240 per cycle was fixed at an amplitude sufficient to com-
 241 pletely elongate the rostrum and generate a tensile load of
 242 1.0 N in the straightened configuration (ca. 20% ultimate
 243 strength), at a frequency of 0.33 Hz. The test was termi-
 244 nated after a period of two weeks – i.e., ca. 400,000 cycles
 245 – when the stress amplitude appeared to reach an asymp-

246 totic minimum. The rostrum behaved viscoelastically,
 247 indicated by hysteresis in the stress-strain relationship
 248 during each cycle. Strain amplitude decreased logarith-
 249 mically with cycle number, and the specimen appeared
 250 to have been deformed plastically and permanently dur-
 251 ing the test. However, after cleaning the specimen in a
 252 24-hour wash with ethanol and water, the rostrum had
 253 returned to its original shape (Fig. 5).

254 While we cannot fully determine the cause for ro-
 255 strum stress relaxation after testing, we speculate that
 256 it arose from the general mechanism associated with cu-
 257 ticle viscoelasticity. The endocuticle is made of aligned
 258 α -chitin nanofibrils whose crystalline structure is enforced
 259 by hydrogen bonds between individual chitin chains and
 260 through the protein matrix along their length. Macro-
 261 scopic viscoelastic behavior results from slippage between
 262 these chains in response to shearing between the chitin
 263 molecules [2, 43, 44]. Repeated strain may have caused
 264 such slippage in the endocuticle of the rostral apex during
 265 the fatigue test. Without sufficient time for the material
 266 to completely relax after deformation, the rostrum would
 267 slowly accumulate strain and deform viscoelastically [40].
 268 After immersion in ethanol and water, however, the cu-
 269 ticle would be sufficiently plasticized to allow the rostrum
 270 to return to its original configuration, thus dissipating
 271 the accumulated strain.

272 The specimen did not show any evidence of fractures,
 273 micro-tears, or shear cusps anywhere in the surface of
 274 the exocuticle. Moreover, the tensile strength of the
 275 tested specimen’s rostrum was consistent with that of
 276 other species members ($F_{max} = 5.02$ N). Surprisingly,
 277 the specimen remained undamaged by the testing. We
 278 therefore conclude that under normal life conditions, re-
 279 peated bending of the rostrum does not exceed the yield
 280 strength of the cuticle.

281 IV. FRACTOGRAPHY OF CURCULIO TEST 282 SPECIMENS

283 In light of the complex failure modes evident in the
 284 fractured specimens, it was not always possible to iden-
 285 tify void nucleation and crack initiation sites. We ob-
 286 served several patterns characteristic of both the micro-
 287 scale behavior of the cuticle and the meso-scale behavior
 288 of the rostrum during uniaxial tensile failure (Fig. 6).
 289 These patterns are described below.

290 In transverse view, the exocuticle consistently pre-
 291 sented a nearly continuous fracture surface. This is char-
 292 acteristic of comparatively brittle failure – presumably
 293 due to the relatively homogeneous arrangement of α -
 294 chitin laminae in the Bouligand structure [25, 26]. The
 295 exocuticle typically appeared to fracture at lower strains
 296 than the endocuticle, with shear-cusp formation evident
 297 both at the fracture surface and across exocuticle adja-
 298 cent to the plane of fracture [45]. Conversely, the endocu-
 299 ticle exhibited severe delamination, off-axis ply-splitting,
 300 and fiber-pulling away from the fracture surface. This

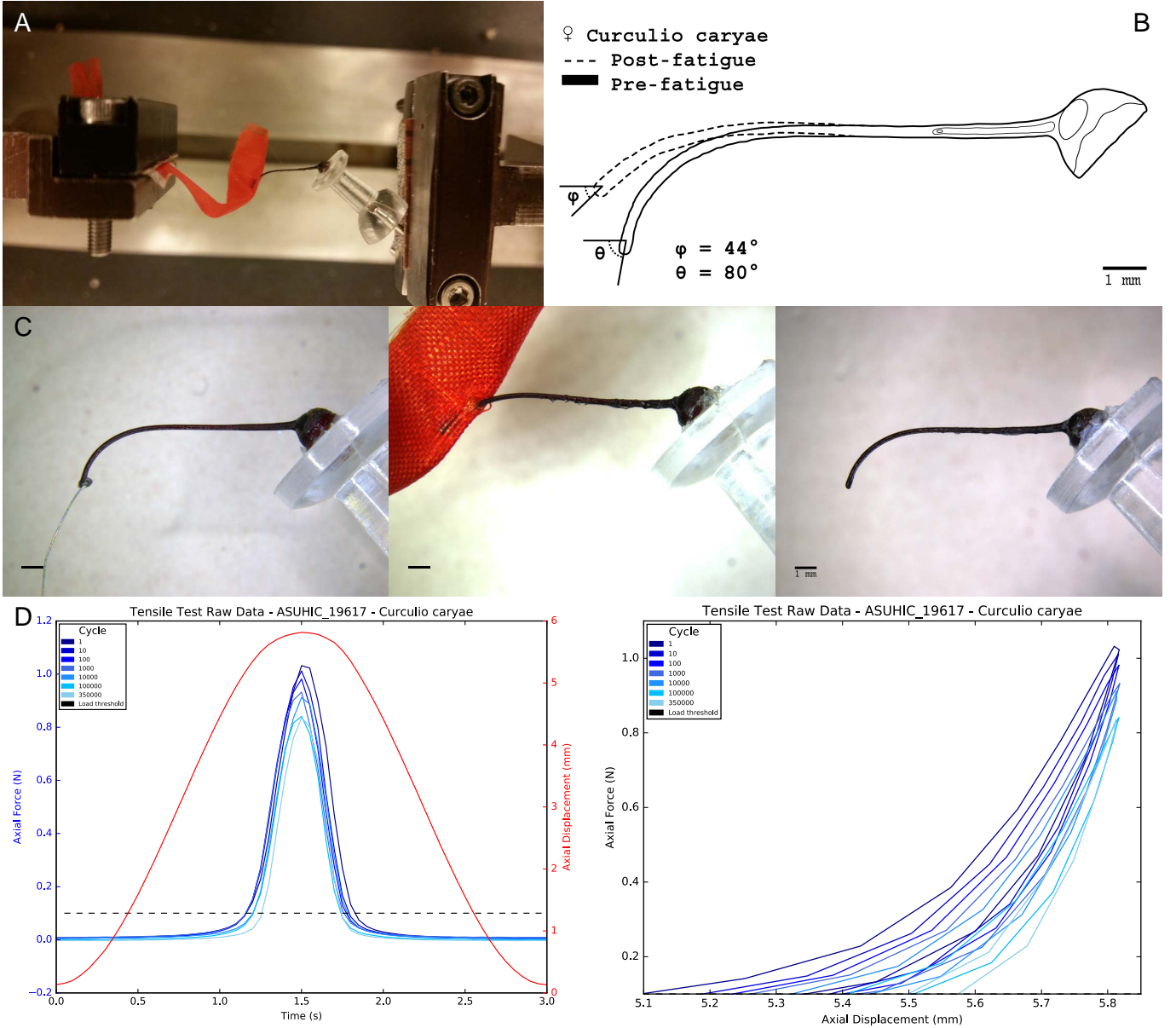


FIG. 5. Fatigue testing of a female *Curculio caryae* rostrum. **a**, Set-up of fatigue testing, with female's head capsule fixed to pedestal and rostrum attached to strip of rip-stop nylon fabric using cyanoacrylate adhesive. Specimen was loaded in tension, as opposed to compression, therefore isolating effect of tension on fatigue behavior of rostrum. **b**, Overlay of pre- and post-fatigue states of head, showing clear (short-term) effect from repeated prescribed strain. **c**, Three-photograph sequence of pre- and post-fatigue states of the rostrum; with left and central panels showing conditions immediately prior to and after testing, respectively, whereas right panel shows head having returned to its original shape after 24 hours off soaking in a water/ethanol mixture. Hence immediate post-fatigue shape is not permanent. **d**, Raw force data (left) and displacement data (right) plots for fatigue test. Displacement data plot shows clear viscoelastic behavior, indicated by hysteresis in stress-strain response of specimen, and exhibits logarithmic decrease stress amplitude over time.

301 is indicative of the relatively high toughness of the uni-
 302 directional α -chitin organization within the macrofibers
 303 [4, 5]. Because the exocuticle of weevils is anchored to
 304 the endocuticle by cross-linking fibers (see [5, 23]), exocu-
 305 ticular shear-cusp formation in uniaxial tension suggests
 306 extension-shear coupling within individual endocuticle
 307 laminae; and further implies that ply-splitting occurred
 308 via mode II fracture between macrofibers at high strain
 309 [32, 33]. We hypothesize that intra-laminar extension-
 310 shear coupling also yielded off-axis, in-plane resultant
 311 forces as a function of lamina orientation angle. Mode
 312 III shearing then occurred between laminae with oppos-
 313 ing in-plane resultant forces, causing the observed inter-
 314 ply delamination. Tensile failure of the macrofiber lam-

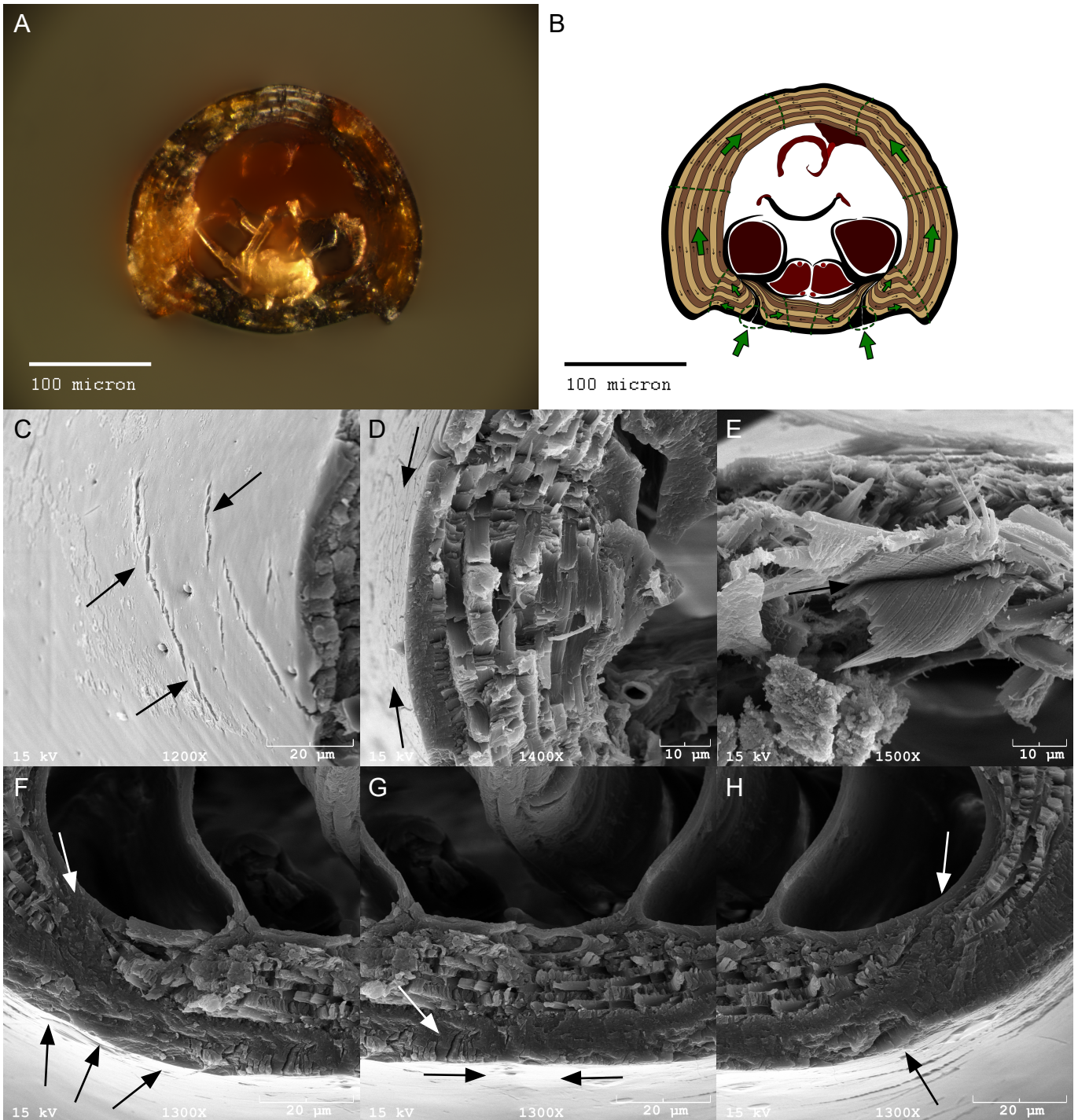


FIG. 6. Fractography of female *Curculio* rostrum. **a**, Light micrograph showing the fracture surface of tensile tested *Curculio caryae* rostrum, displaying typical failure mode; illustrated in **(b)**: Small, black arrows indicate the winding direction of macrofiber lamina; green arrows and dotted lines indicate the direction of crack. Scanning electron micrographs highlight: **(c)** shear cusp formation; **(d)** tensile failure and off-axis macrofiber fiber-pulling; **(e)** interlaminar delamination; **(f-h)** crack formation near invaginated exocuticle; and **(g)** ventral crack-front coalescence and shear cusp formation.

315 inae would ultimately occur via mixed-mode I/II – i.e., 319 At the meso-scale, most specimens fractured along a
316 transverse tension/intra-laminar shear – fracture, due to 320 single plane across and between the occipital sulci, which
317 an increase in applied stress caused by ply-splitting in 321 are cuticular invaginations that traverse the entire length
318 adjacent laminae [45]. 322 of the rostrum [13, 17]. These sulci increase the volume

323 fraction of exocuticle in the ventral part of the snout.
 324 They contain large interfaces ideal for void nucleation
 325 (Fig. 6). The exocuticle of the occipital sulci usually
 326 displayed shear cusps oriented outward from the center
 327 of the invagination, and continuing dorsolaterally and
 328 ventromedially. Ventrally, the cusps converged toward
 329 a prominent scarp where the crack fronts joined. This
 330 scarp was often obscured by delaminated endocuticular
 331 macrofibers in specimens with large cross-sectional areas
 332 of endocuticle,

333 The first layer of endocuticle usually fractured along
 334 the same plane as the exocuticle. Ventrally, the endocu-
 335 ticle laminae typically converged toward a scarp-like re-
 336 gion characterized by severe delamination and numerous
 337 de-bonded macrofibers. Moreover, macrofibers aligned
 338 with the direction of crack propagation exhibited exten-
 339 sive ply-splitting with intermittent transverse shearing.
 340 In contrast, macrofibers oriented against the direction of
 341 crack propagation primarily displayed fracture by trans-
 342 verse shear along the plane of ply-splitting in adjacent
 343 laminae. Because the laminae form a cylinder, contralat-
 344 eral fibers in the same lamina display opposing fracture
 345 modes. The ventrolateral surfaces often exhibited exten-
 346 sive inter-ply delamination and fiber de-bonding in scarp-
 347 like prominences. This is likely due to a combination of
 348 tensile failure and shearing along the dorsally-radiating
 349 crack front. Dorsally, the coalescent crack fronts often
 350 caused significant de-bonding and ply-splitting, followed
 351 by broom-like tensile failure. In some specimens, the con-
 352 tralateral crack fronts were out of plane and coalesced via
 353 transverse shear through a large dorsal section of cuticle.
 354 Based on these failure patterns, we hypothesize that
 355 the exocuticle-rich occipital sulci are the most likely site
 356 for the initiation of void nucleation and catastrophic fail-
 357 ure of the integrated rostral cuticle in cross section, as
 358 illustrated in Fig. 6. Structural failure would take place
 359 as cracks propagate through the endocuticle from these
 360 sutures, and ultimately penetrating the entire thickness
 361 of the laminate [13]. Although other, more complex fail-
 362 ure modes have been observed, we posit that in live spec-
 363 imens this is the most likely mechanism of tensile failure
 364 because typical bending behavior generates tension *only*
 365 along the ventral surface of the rostrum.

366

V. CONCLUSIONS

367 The rostrum of *Curculio* is characterized by a discon-
 368 tinuous composite profile. The cuticle is strongly differ-
 369 entiated in terms of relative layer thicknesses and ori-
 370 entation angles along an anterior-posterior gradient. These
 371 modifications are sufficient to achieve a marked reduc-
 372 tion in the effective membrane and flexural moduli of
 373 the cuticle – 72% and 60%, respectively – in constitu-
 374 tive models based on CLPT, thereby accounting for the
 375 observed flexibility of the rostral apex in live specimens.
 376 However, the reductions can only be realized with *both*
 377 modifications to the cuticle, which have a non-additive

378 effect on cuticle elasticity. *Curculio* females require both
 379 modifications to function properly during oviposition.

380 Likewise, tensile and fatigue testing reveal a trade-off
 381 between stiffness and fracture resistance – measured by
 382 ultimate strain and toughness – mediated by the relative
 383 proportion of endocuticle in the laminate. The altered
 384 composite profile of the cuticle in the rostral apex makes
 385 the rostrum simultaneously more flexible and fracture re-
 386 sistant, permitting the structure to be flexed without ex-
 387 ceeding the elastic limits of the cuticle.

388 This is to our knowledge the first time in arthropods
 389 that the composite profile of the cuticle has been re-
 390 lated to a gradient in elasticity and tensile performance
 391 across a cuticular structure. Because these associations
 392 are independent of species membership, we posit that
 393 the behavior of the cuticle is consistent across the genus.
 394 Rostral flexibility is achieved exclusively in all *Curculio*
 395 species through a modified cuticle lay-up. This inference
 396 raises the intriguing possibility that a single ancestral
 397 shift in cuticle organization at the rostral apex – yielding
 398 higher flexibility and tensile strength – enabled the evo-
 399 lutionary “exploration” of a large morphospace region,
 400 promoting the high species-level diversity of this lin-
 401 eage.

402 Based on fractographic analysis of the test specimens,
 403 we infer that the exocuticle exhibits brittle fracture at
 404 a comparatively low strain, due to shearing between the
 405 endocuticle macrofibers to which it is anchored. These
 406 macrofibers fail at higher strain, mediated by mixed-
 407 mode shearing and tensile fracture within and between
 408 laminae. This outcome is consistent with behavior shown
 409 in previous studies, as well as theoretical consideration
 410 of cuticle microstructure in CLPT. The latter predicts
 411 extension shear-coupling ($A_{16}, A_{26} \neq 0$) for individual
 412 off-axis macrofiber laminae [32, 33].

413 Our results imply that fracture initiation occurs in the
 414 comparatively brittle exocuticle. The reduction in exo-
 415 cuticle thickness in the rostral apex might serve to mit-
 416 iate crack formation in rostral bending. Based on this
 417 pattern of fracture behavior, we identified the exocuticle-
 418 rich occipital suture as a common point of void nucleation
 419 and crack initiation. From an evolutionary perspective,
 420 these findings reveal an unexpected morphological source
 421 of constraint on rostral flexibility, raising the intriguing
 422 possibility that this system evolved primarily via nega-
 423 tive selection of fracture, rather than positive selection
 424 of flexibility. In particular, the cuticle is invaginated in
 425 precisely the portion of the snout that experiences the
 426 greatest degree of tension during antero-dorsal flexion.
 427 The doubly-thick exocuticle in the invagination thus cre-
 428 ates an unavoidable, brittle weak-point in an otherwise
 429 endocuticle-dominated rostral apex. This constraint – in
 430 conjunction with the minimization of exocuticle thickness
 431 in the rostral apex and the increased toughness derived
 432 from a thickened endocuticle – lead us to consider that
 433 avoidance of catastrophic structural failure has been a
 434 driving selective pressure in the evolution of the female
 435 *Curculio* rostrum.

VI. METHODS

437 Methods, including statements of data availability and
 438 any associated accession codes and references, are avail-
 439 able in the online version of this paper.

440

REFERENCES

- 441 [1] Jansen, M. A., Singh, S. S., Chawla, N., & Franz, N.
 442 M. A multilayer micromechanical model of the cuticle of
 443 *Curculio longinasus* Chittenden, 1927 (Coleoptera: Cur-
 444 culionidae). *J. Struct. Biol.* **195**: 2, 139–158, (2016).
- 445 [2] Vincent, J. F. V. & Wegst, U. G. K. Design and mech-
 446 ical properties of insect cuticle. *Arthropod Struct. Dev.*
 447 **33**:3, 187–199, (2004).
- 448 [3] Hepburn, H. R. & Ball, A. On the structure and me-
 449 chanical properties of beetle shells. *J. Mater. Sci.* **8**:5,
 450 618–623, (1973).
- 451 [4] van de Kamp, T. & Greven, H. On the architecture of
 452 beetle elytra. *Entomol. Heute* **22**, 191–204, (2010).
- 453 [5] van de Kamp, T., Riedel, A. & Greven, H. Micromorphol-
 454 ogy of the elytral cuticle of beetles, with an emphasis on
 455 weevils (Coleoptera : Curculionoidea) *Arthropod Struct.*
 456 *Dev.* **45**:1, 14–22, (2016).
- 457 [6] Neville, A. C., Parry, D. A. & Woodhead-Galloway, J.
 458 The chitin crystallite in arthropod cuticle. *J. Cell Sci.*
 459 **21**:1, 73–82, (1976).
- 460 [7] Amini, S., Tadayon, M., Idapalapati, S., and Miserez, A.
 461 The role of quasi-plasticity in the extreme contact dam-
 462 age tolerance of the stomatopod dactyl club *Nat. Mater.*
 463 **14**:9, 943–950, (2015).
- 464 [8] McCullough, E. L., Tobalske, B. W., and Emlen, D. J.
 465 Structural adaptations to diverse fighting styles in sexu-
 466 ally selected weapons *Proc. Natl. Acad. Sci. USA* **111**:40,
 467 14484–14488, (2014).
- 468 [9] McCullough, E. L. Mechanical limits to maximum
 469 weapon size in a giant rhinoceros beetle *Proc. R. Soc.*
 470 *B* **281**, 20140696, (2014).
- 471 [10] Dirks, J., Parle, E., and Taylor, D. Fatigue of insect cu-
 472 ticle *J. Exp. Biol.* **216**:10, 1924–1927, (2013).
- 473 [11] Dirks, J. and Taylor, D. Fracture toughness of locust
 474 cuticle *J. Exp. Biol.* **215**:9, 1502–1508, (2012).
- 475 [12] *International Code of Zoological Nomenclature* Fourth
 476 Edition. (The International Trust for Zoological Nomen-
 477 cature, London, 1999).
- 478 [13] Davis, S. R. *Morphology, phylogeny, and evolutionary*
 479 *development in the weevils (Insecta: Coleoptera: Cur-*
 480 *culionoidea)* (Ph.D. thesis, University of Kansas, 2014).
- 481 [14] Singh, S. S., Jansen, M. A., Franz, N. M., and Chawla,
 482 N. Microstructure and nanoindentation of the rostrum of
 483 *Curculio longinasus* Chittenden, 1927 (Coleoptera: Cur-
 484 culionidae) *Mater. Charact.* **118**, 206–211, (2016).
- 485 [15] Toju, H. and Sota, T. Imbalance of predator and prey
 486 armament: geographic clines in phenotypic interface and
 487 natural selection *Am. Nat.* **167**:1, 105–117, (2006).
- 488 [16] Gibson, L. P. Monograph of the genus *Curculio* in the
 489 New World (Coleoptera: Curculionidae). Part I. United
 490 States and Canada *Misc. Publ. Entomol. Soc. Am.* **6**,
 491 239–285, (1969).
- 492 [17] Dennell, R. The structure and function of the mouth-
 493 parts, rostrum and fore-gut of the weevil *Calandra gra-*
 494 *naria* L. *Phil. Trans. R. Soc. Lond. B* **231**:581, 247–291,
 495 (1942).
- 496 [18] Morimoto, K. and Kojima, H. Morphologic charac-
 497 ters of the weevil head and phylogenetic implica-
 498 tions (Coleoptera, Curculionoidea) *Esakia* **43**, 133–169,
 499 (2003).
- 500 [19] Ting, P. C. Feeding mechanisms of weevils, their func-
 501 tion, and relationship to classification *Mon. Bull. Dep.*
 502 *Agric. State Calif.* **22**, 161–165, (1933).
- 503 [20] Ting, P. C. The mouth parts of the coleopterous group
 504 *Rhynchophora* *Microentomology* **1**, 93–114, (1936).
- 505 [21] Aguirre Uribe, L. A. *Biology of the immature stages of*
 506 *the pecan weevil Curculio caryaev (Horn) and oviposition*
 507 *habits of the adult weevil* (Ph.D. thesis, Texas A & M
 508 University, 1978).
- 509 [22] Moffett, M. Life in a nutshell *Natl. Geogr. Mag.* **176**,
 510 783–784, (1989).
- 511 [23] Longhai, L. et al. Microstructure and mechanical
 512 properties of rostrum in *Cyrtotrachelus longimanus*
 513 (Coleoptera: Curculionidae) *Anim. Cells Syst.* **21**:3,
 514 199–206, (2017).
- 515 [24] Matsumura, Y., Kovalev, A. E., and Gorb, S. N. Pen-
 516 etration mechanics of a beetle intromittent organ with
 517 bending stiffness gradient and a soft tip, *Sci. Adv.* **3**:12,
 518 eaao5469, (2017).
- 519 [25] Nikolov, S. et al. Robustness and optimal use of design
 520 principles of arthropod exoskeletons studied by ab initio-
 521 based multiscale simulations. *J. Mech. Behav. Biomed.*
 522 *Mater.* **4**:2, 129–145, (2011).
- 523 [26] Nikolov, S. et al. Revealing the design principles of high-
 524 performance biological composites using Ab initio and
 525 multiscale simulations: The example of lobster cuticle.
 526 *Adv. Mater.* **22**:4, 519–526, (2010).
- 527 [27] Blackwell, J. and Weih, M. Structure of chitin-protein
 528 complexes: ovipositor of the ichneumon fly *Megarhyssa*.
 529 *J. Mol. Biol.* **137**:1, 49–60, (1980).
- 530 [28] Bouligand, Y. Twisted fibrous arrangements in biological
 531 materials and cholesteric mesophases. *Tissue Cell* **4**:2,
 532 189–217, (1972).
- 533 [29] Vincent, J. F. V. *Structural biomaterials* (Halsted Press,
 534 New York, 1982).
- 535 [30] Cheng, L., Wang, L., & Karlsson, A. M. Mechanics-based
 536 analysis of selected features of the exoskeletal microstruc-
 537 ture of *Popillia japonica*. *Mater. Res.* **24**:11, 3253–3267,
 538 (2009).
- 539 [31] Leopold, R. A., Newman, S. M., and Helgeson, G. A com-
 540 parison of cuticle deposition during the pre-and poste-
 541 closion stages of the adult weevil, *Anthomous grandis*
 542 BOHEMAN (Coleoptera: Curculionidae) *Int. J. Insect*
 543 *Morphol. and Embryol.*, **21**:1, 37–62, (1992).
- 544 [32] Reddy, J. N. *Mechanics of laminated composite plates*
 545 and shells: theory and analysis (CRC Press, Philadel-

- 546 phia, 2004).
- 547 [33] Jones, R. M. *Mechanics of composite materials* (CRC
548 press, Philadelphia, 2014).
- 549 [34] Hughes, J. and Vogler, A. P. The phylogeny of acorn
550 weevils (genus *Curculio*) from mitochondrial and nuclear
551 DNA sequences: the problem of incomplete data *Mol.*
552 *Phylogenet. Evol.* **32:2**, 601–615, (2004).
- 553 [35] Bonal, R. et al. Diversity in insect seed parasite guilds at
554 large geographical scale: the roles of host specificity and
555 spatial distance *J. Biogeogr.* **43:8**, 1620–1630, (2016).
- 556 [36] Hughes, J. and Vogler, A. P. Ecomorphological adapta-
557 tion of acorn weevils to their oviposition site *Evolution*
558 **58:9**, 1971–1983, (2004).
- 559 [37] Bonal, R., Espelta, J. M., and Vogler, A. P. Complex se-
560 lection on life-history traits and the maintenance of vari-
561 ation in exaggerated rostrum length in acorn weevils *Oe-*
562 *cologia* **167:4**, 1053–1061, (2011).
- 563 [38] Klocke, D. & Schmitz, H. Water as a major modulator
564 of the mechanical properties of insect cuticle. *Acta Bio-*
565 *mater.* **7**, 2935–2942 (2011).
- 566 [39] Mihai, L. A. and Goriely, A. How to characterize a non-
567 linear elastic material? A review on nonlinear constitu-
568 tive parameters in isotropic finite elasticity *Phil. Trans.*
569 *R. Soc. Lond. A* **473:2207**, 20170607, (2017).
- 570 [40] Münster, S. et al. Strain history dependence of the
571 nonlinear stress response of fibrin and collagen net-
572 works *Proc. Natl. Acad. Sci. USA* **110:30**, 12197–12202,
573 (2013).
- 574 [41] Felsenstein, J. Phylogenies and the comparative method
575 *Am. Nat.* **125:1**, 1–15, (1985).
- 576 [42] Revell, L. J. Phylogenetic signal and linear regression on
577 species data *Methods Ecol. Evol.* **1:4**, 319–329, (2010).
- 578 [43] Beament, J. W. L., Treherne, J. E., and Wigglesworth,
579 V. B. *Advances in insect physiology* Volume 4 (Academic
580 Press Inc., London, 1967).
- 581 [44] Sun, J. Y. et al. Differential constitutive equation of ely-
582 tra cuticle by nanoindentation *Adv. Mater. Res.*, **343**,
583 1133–1139, (2012).
- 584 [45] Greenhalgh, E. *Failure analysis and fractography of poly-*
585 *mer composites* (CRC Press, Boca Raton, 2009).

AUTHOR CONTRIBUTIONS

601 M.A.J. conducted sectioning and staining, microscopy
602 and imaging, tensile and fatigue testing, statistical
603 analysis, and participated in manuscript preparation.
604 J.W. conducted tensile and fatigue testing and partic-
605 ipated in manuscript preparation. N.C. facilitated mi-
606 croscopy, tensile and fatigue testing, and participated
607 in manuscript preparation. N.M.F. facilitated specimen
608 acquisition and imaging and participated in manuscript
609 preparation.

ADDITIONAL INFORMATION

611 612 Supplementary information is available in the online
613 version of the paper. Reprints and permissions infor-
614 mation is available online at www.nature.com/reprints.
615 Correspondence and requests for materials should be ad-
616 dressed to M.A.J.

COMPETING FINANCIAL INTERESTS

617 618 The authors declare no competing financial interests.

ACKNOWLEDGMENTS

586 The authors are grateful to Robert Anderson (CMNC),
587 Lourdes Chamorro (USNM), and Charlie O'Brien
588 (CWOB) for their assistance and provision of *Curculio*
589 specimens used in this study. The authors thank Sal-
590 vatore Anzaldo, Andrew Johnston, Brian Reilly, Sangmi
591 Lee, and other Arizona State University Hasbrouck In-
592 sect Collection (ASUHIC) members for their assistance
593 in procuring, treating, and maintaining specimen loans
594 upon entry into the ASUHIC. The authors would also
595 like to thank David Lowry (ASU CLAS Bioimaging Cen-
596 ter) for his training and assistance with resin embed-
597 ding, scanning electron microscopy, and microtomogra-
598 phy; and Salvatore Anzaldo for his assistance with histo-
599 logical staining.

619

METHODS

620

Specimen acquisition and taxon sampling

621 Specimens for use in tensile and fatigue testing came
 622 from the Hasbrouck Insect Collection at Arizona State
 623 University [ASUHIC]. This set of specimens was supple-
 624 mented with material housed in the following collections,
 625 using the codens of Arnett et al. [46]:

626 CMNC: Canadian Museum of Nature Collection, Ottawa,
 627 Ontario, Canada

628 USNM: National Museum of Natural History, Washington,
 629 D.C., USA

630 Cold fracture, semi-thin sectioning, and tensile testing
 631 were conducted on randomly chosen female specimens be-
 632 longing to six *Curculio* species obtainable through field
 633 work in the southwestern United States and northwest-
 634 ern Mexico. Taxon sampling was targeted to represent
 635 a mixture of disparate radiations and sister taxa with
 636 a variety of rostral morphotypes in accordance with the
 637 phylogenetic hypotheses of Hughes et al. [34, 36] and
 638 Bonal et al. [35]. The six species of *Curculio* used herein
 639 are (in alphabetical sequence): *Curculio caryae* (Horn,
 640 1873), *Curculio humeralis* (Casey, 1897), *Curculio pro-*
boscideus Fabricius, 1775, *Curculio sulcatulus* (Casey,
 642 1897), *Curculio uniformis* (LeConte, 1857), and *Cur-*
culio victoriensis (Chittenden, 1904). Specimens were
 644 identified to taxonomic (species) concepts using [16] and
 645 other resources.

646

Histological sectioning

647 To illustrate the relative proportions of the cuti-
 648 cle regions in cross-section, serial semi-thin sectioning
 649 was conducted on exemplary female specimens of *Cur-*
culio humeralis and *Curculio longinasus* Chittenden,
 651 1927. Live specimens of both species were collected into
 652 95% ethanol for preservation. A female specimen was
 653 selected; and the rostrum was separated from the head
 654 capsule with a fine-edged razor blade. The apical 1/4th
 655 of the rostrum was also removed and then discarded. The
 656 remaining portion of the rostrum and the head capsule
 657 were then embedded in EMbed812, as follows.

658 The cuticle was first immersed in acetone for 24 hours,
 659 and then transferred to a 2:1 mixture of acetone to epoxy
 660 resin. Samples remained at 21°C for 12 hours on a shaker
 661 table to prevent hardening. They were then transferred
 662 into a 1:1 mixture of acetone to resin, followed by a 1:2
 663 mixture (each for 12 hours and at 21°C on a shaker ta-
 664 ble), before finally being placed into a silicone mold with
 665 pure resin. The mold was placed into an oven heated
 666 to 38°C, and the resin was allowed to cure for 24 hours.
 667 The resulting blocks were machined to prepare the apical
 668 surface of each sample for microtomy.

669 A Leica Ultracut R Microtome and diamond knife were
 670 used to expose a cross-section (transverse plane) of the
 671 apical and basal portions of the rostrum and to remove
 672 excess material. Semi-thin sections (0.5 µm thick) were
 673 kept and stained with toluidine-blue-borax for light mi-
 674 croscopy and imaging.

Cold-fracture of specimens

675 676 Two pinned female specimens of each *Curculio* species
 677 were selected at random and retained for cold-fracturing
 678 of the rostrum. The heads of the specimens were re-
 679 moved and cleaned using a 95% ethanol solution and a
 680 thin paintbrush. Any muscles protruding from the occip-
 681 ital foramen were removed with a fine-edged razor blade.
 682 The antennae were removed directly using forceps to pull
 683 the scape (basal section of antenna) from the antennal
 684 insertion. Cleaned specimens were stored at -80°C for
 685 24 hours, then fractured using forceps over a chilled alu-
 686 minum block. To fracture each specimen, the head cap-
 687 sule and rostrum were each gripped firmly in a pair of
 688 forceps. The forceps were then sharply rotated to frac-
 689 ture the base of the snout via dorsal flexion. The rostrum
 690 was fractured a second time, after separation from the
 691 head capsule, using the same procedure. The segmented
 692 specimens were then placed into individual glass vials to
 693 protect the fracture surfaces from contamination prior to
 694 microscopy.

695

Tensile and fatigue testing

696 697 *Force-controlled loading to failure.* Five female spec-
 698 imens of each *Curculio* species were randomly allocated
 699 for use in tensile testing. The head of each specimen was
 700 removed, cleaned, and prepared as described above in the
 701 cold-fracture protocol. To avoid destroying the delicate,
 702 brittle specimens when gripping the ends of each head,
 703 a method was devised to create solid handles that could
 704 be clamped tightly into grips without risk of damage to
 705 the cuticle.

706 For each head, four 1 cm² strips of gaffer tape were cut;
 707 these were used as gripping and mounting points for the
 708 specimen. A strip of tape would be laid flat, with a large
 709 drop of cyanoacrylate glue placed upon the upturned sur-
 710 face. The curved portion of the snout was then placed
 711 into the drop, such that the straight portion of the ro-
 712 strum was aligned perpendicular to the edge of the strip.
 713 Hardening of the cyanoacrylate effectively embedded the
 714 curved portion of the snout in a solid mass, isolating a
 715 straight section of the snout – from the base to a point
 716 distad of the apex of the scrobe – for testing. A second
 717 strip of tape was fixed over this mass with an additional
 718 layer of cyanoacrylate to provide a dorsal gripping sur-
 719 face for the mass. A small mark was made to indicate
 720 the extent of the head inside the mass. This embedding
 procedure was repeated for the head capsule, resulting in

721 a finished specimen with anterior and posterior handles
 722 for testing.

723 Prior to testing, each specimen was placed in de-
 724 ionized water for 24 hours to allow full saturation of the
 725 cuticle, simulating the condition of live tissue [38]. Once
 726 removed for testing, the specimen was gripped using the
 727 cyanoacrylate handles at the marked locations immedi-
 728 ately beyond the anterior margin of the rostrum and the
 729 posterior margin of the head capsule. The exposed sec-
 730 tion of the snout was coated in petroleum jelly using a
 731 cotton swab to prevent loss of moisture and stiffening of
 732 the specimen during the test. Specimens were loaded in
 733 a Tryton 250 Microforce Testing System equipped with
 734 a 5N load cell and mechanical clamp grip. All specimens
 735 were subjected to force-controlled uniaxial tension at a
 736 rate of $1.0 \text{ gf} \cdot \text{s}^{-1}$ until failure, with a sampling interval
 737 of 0.1 s. Engineering stresses ($\sigma_0 = F/A_0$) and strains
 738 ($\epsilon_0 = \Delta l/l_0$) were reported only for specimens that did
 739 not fracture due to strain accumulation at the interface
 740 between the rostrum and the cyanoacrylate handles.

741 *Displacement-controlled cyclic loading.* To confirm
 742 that repeated, complete extension of a strongly curved
 743 rostrum would not result in fracture of the cuticle, a rep-
 744 resentative female specimen of *Curculio caryae* was allo-
 745 cated for fatigue testing. The head capsule of the spec-
 746 imen was fixed to a push-pin using cyanoacrylate glue.
 747 This served as a pedestal and gripping location for the
 748 posterior portion of the specimen. The apex of the ros-
 749 trum was fixed to a strip of ripstop nylon fabric equal
 750 in length to the head, using cyanoacrylate glue. As with
 751 tensile testing, the specimen was placed in de-ionized wa-
 752 ter for 24 hours, then coated in petroleum jelly using a
 753 cotton swab immediately prior to load cycling.

754 The end of the fabric was gripped and used to elon-
 755 gate the rostrum in tension by pulling on the fabric, thus
 756 isolating the effect of tension on the fatigue life of the ros-
 757 tral cuticle. In this way, the rostrum would return to its
 758 original configuration in a spring-like manner, as in liv-
 759 ing specimens, rather than being forced to return to the
 760 initial position. The rostrum was aligned such that com-
 761 plete elongation of the curved section would take place in
 762 tension, with minimal off-axis deflection of the un-curved
 763 section. The specimen was subjected to displacement-
 764 controlled loading sufficient to fully extend the rostrum
 765 and generate a load stress of 1 N, or approximately 20%
 766 of the tensile strength of the species average. Load cy-
 767 cling took place at a rate of 0.33Hz, and was continued
 768 for 14 days – i.e., 400,000 cycles – until the tensile stress
 769 in the sample approached an asymptotic minimum.

770 Once the test was concluded, the specimen was placed
 771 in a 50% ethanol solution for 24 hours to clean the
 772 petroleum jelly from the rostrum. The specimen was
 773 examined for surface fractures and micro-tears, then sub-
 774 jected to tensile testing via the same protocol as the other
 775 specimens to assess whether the cuticle had begun to fa-
 776 tigue.

Specimen imaging and microscopy

778 The fracture surfaces of cold-fractured specimens were
 779 examined using scanning electron microscopy to charac-
 780 terize the composite profile and microstructure of the
 781 rostrum. Fracture behavior of tensile testing specimens
 782 was assessed using both light microscopy and SEM to
 783 image the fracture surfaces of the specimens in trans-
 784 verse view. Electron microscopy was conducted using
 785 a JEOL JSM6300 scanning electron microscope. Light
 786 microscopy was conducted using a Leica M205 C stere-
 787 omicroscope and attached computer running the software
 788 Leica Application Suite (LAS); as well as a Visionary
 789 Digital Passport II system using a Canon EOS Mark 5D
 790 II camera outfitted with interchangeable macro lenses.
 791 Specimen length, layer thicknesses, macrofiber orienta-
 792 tion angles, and cross-sectional areas were measured in
 793 the LAS and in Adobe Illustrator, using pixel-wise mea-
 794 surements multiplied by a scaling factor for the image.

Constitutive modeling of the cuticle

795 *General approach.* The effective uni-axial membrane
 796 and transverse flexural elastic moduli of idealized cuti-
 797 cle organizations, representing both the rostral apex and
 798 head capsule, were estimated using Classical Laminate
 799 Plate Theory (CLPT). For general information on this
 800 approach see [32, 33]. The composite profiles of both
 801 types of cuticle were idealized using the layer thicknesses
 802 and stacking sequences observed in *Curculio longinasus*.
 803 This particular species was chosen because we derived
 804 the effective elastic constants of the individual compo-
 805 nents of the cuticle in previous work [1, 14]. In addition,
 806 *Curculio longinasus* exhibits a profile that is typical and
 807 representative for the genus *Curculio*, based on examina-
 808 tion of the six species used for tensile testing.

809 For *Curculio longinasus* the total thickness of the
 810 cuticle in the head and rostrum is roughly 50 μm ,
 811 as in most specimens of the other examined species.
 812 In the head capsule, the exocuticle occupies between
 813 30-50% of the through-thickness of the laminate, with
 814 the remaining thickness nearly evenly divided between
 815 12 layers of endocuticle. We use the maximum (50% of
 816 through-thickness, or 25 μm) for the model, since the
 817 cuticle appears to deviate from this value only in regions
 818 with sulci (grooves), pores, and other scattered features
 819 of the surface sculpture. The macrofiber laminae of
 820 the endocuticle were assigned a stacking sequence of
 821 $0^\circ, 90^\circ, 30^\circ, -60^\circ, 60^\circ, -30^\circ, 90^\circ, 0^\circ, -60^\circ, 30^\circ, -30^\circ, 60^\circ$;
 822 thereby representing pairs of orthogonal plies stacked at
 823 a constant rotation angle of 30° , in approximation of the
 824 living tissue.

825 In the rostral apex, the exocuticle is reduced to a thin
 826 shell approximately 5 μm in thickness, or 10% of the total
 827 cuticle thickness. The endocuticle displays a more com-
 828 plex pattern of layer thicknesses in the rostral apex than
 829 in the head capsule. Each of the eight outermost layers

are of nearly equal thickness to the exocuticle (5 μm), whereas the four innermost layers have a combined thickness equal to that of the exocuticle or to a single layer of outer endocuticle ($h_{\text{outer}} = 5 \mu\text{m}$, $h_{\text{inner}} = 1.25 \mu\text{m}$). The stacking sequence with respect to the longitudinal axis of the rostrum forms an antisymmetric angle-ply laminate of $\pm 45^\circ$.

To assess the individual contributions of layer thickness and stacking angle sequence to cuticle flexibility in the rostral apex, two hypothetical cuticle lay-ups were modeled – each with only one of the modifications present in the cuticle of the rostral apex. The first of these models has the layer thicknesses of the rostral apex, but fiber orientations of the head capsule; whereas the second has the fiber orientations of the rostral apex, but the layer thicknesses of the head capsule.

Because these laminates are not symmetric, each has a bending-extension coupling matrix $[B]$ populated with non-zero terms; thus complicating the calculation of effective in-plane elastic moduli. To circumvent this difficulty and enable meaningful comparisons between each laminate, all of the lay-ups are reflected about their inner surface. This effectively doubles their thickness while producing a balanced, symmetric laminate with no coupling between bending and extension (i.e., $[B] = 0_{3,3}$). Estimation of in-plane elastic constants from the extension($[A]$) and bending ($[D]$) matrices is described in detail below. The program Matlab R2018b was used to numerically evaluate the final values of the effective elastic constants [47].

Classical Laminate Plate Theory. We begin by calculating the 2D reduced stiffness matrix for each part of the cuticle. For orthotropic materials with the principal axes parallel to the ply edges, the reduced stiffness matrix is defined as follows:

$$[Q] = \begin{bmatrix} Q_{11} & Q_{12} & 0 \\ Q_{21} & Q_{22} & 0 \\ 0 & 0 & Q_{66} \end{bmatrix}, \quad (1)$$

where:

$$\begin{aligned} Q_{11} &= \frac{E_1}{1 - \nu_{12}\nu_{21}}, \\ Q_{12} &= \frac{E_1\nu_{21}}{1 - \nu_{12}\nu_{21}} = Q_{21}, \\ Q_{21} &= \frac{E_2\nu_{12}}{1 - \nu_{12}\nu_{21}} = Q_{12}, \\ Q_{22} &= \frac{E_2}{1 - \nu_{12}\nu_{21}}, \\ Q_{66} &= G_{12}. \end{aligned} \quad (2)$$

For each layer k , the reduced stiffness matrix is transformed to account for the layer orientation angle θ within the laminate coordinate system, yielding a reduced transformed stiffness matrix according to:

$$[\bar{Q}] = [T]^{-1}[Q][T]^{-T}, \quad (3)$$

where the transformation matrix $[T]$ is defined as:

$$[T] = \begin{bmatrix} \cos^2 \theta & \sin^2 \theta & 2 \cos \theta \sin \theta \\ \sin^2 \theta & \cos^2 \theta & -2 \cos \theta \sin \theta \\ -\cos \theta \sin \theta & \cos \theta \sin \theta & \cos^2 \theta - \sin^2 \theta \end{bmatrix}. \quad (4)$$

Using the lay-ups specified for each type of cuticle described above, we calculate the extensional stiffness matrix $[A]$, bending stiffness matrix $[D]$, and bending-extension coupling matrix $[B]$ for each laminate consisting of n layers at a distance z from the laminate mid-plane. The elements of these matrices can be identified according to:

$$\begin{aligned} A_{ij} &= \sum_{k=1}^n (\bar{Q}_{ij})_k (z_k - z_{k-1}), \\ B_{ij} &= \frac{1}{2} \sum_{k=1}^n (\bar{Q}_{ij})_k (z_k^2 - z_{k-1}^2), \\ D_{ij} &= \frac{1}{3} \sum_{k=1}^n (\bar{Q}_{ij})_k (z_k^3 - z_{k-1}^3). \end{aligned} \quad (5)$$

These stiffness matrices respectively relate vectors of resultant forces $\{N\}$ and bending moments $\{M\}$ to mid-surface strains and curvatures $\{\epsilon^\circ\}$ and $\{\kappa\}$ in the laminate, according to the following relationship:

$$\begin{Bmatrix} \{N\} \\ \{M\} \end{Bmatrix} = \begin{bmatrix} [A] & [B] \\ [B] & [D] \end{bmatrix} \begin{Bmatrix} \{\epsilon^\circ\} \\ \{\kappa\} \end{Bmatrix}. \quad (6)$$

For symmetric laminates, $[B] = 0_{3,3}$, and therefore:

$$\begin{aligned} \{N\} &= [A]\{\epsilon^\circ\}, \\ \{M\} &= [D]\{\kappa\}, \end{aligned} \quad (7)$$

or, in expanded form:

$$\begin{aligned} \begin{Bmatrix} N_{xx} \\ N_{yy} \\ N_{xy} \end{Bmatrix} &= \begin{bmatrix} A_{11} & A_{12} & A_{16} \\ A_{21} & A_{22} & A_{26} \\ A_{61} & A_{62} & A_{66} \end{bmatrix} \begin{Bmatrix} \epsilon_{xx}^\circ \\ \epsilon_{yy}^\circ \\ \gamma_{xy} \end{Bmatrix}, \\ \begin{Bmatrix} M_{xx} \\ M_{yy} \\ M_{xy} \end{Bmatrix} &= \begin{bmatrix} D_{11} & D_{12} & D_{16} \\ D_{21} & D_{22} & D_{26} \\ D_{61} & D_{62} & D_{66} \end{bmatrix} \begin{Bmatrix} \kappa_{xx} \\ \kappa_{yy} \\ \kappa_{xy} \end{Bmatrix}. \end{aligned} \quad (8)$$

If we make the simplifying assumptions [32, 33] that (1) the laminate experiences pure axial loading and transverse bending (i.e., $N_{yy} = N_{xy} = 0$ and $M_{yy} = M_{xy} = 0$, respectively), and (2) the laminate is a beam of sufficiently high aspect ratio to minimize the Poisson

effect and anisotropic shear coupling (i.e., below we effectively let $A_{12}^* = A_{16}^* = 0$ and $D_{12}^* = D_{16}^* = 0$), then we can calculate the in-plane effective flexural and axial Young's moduli of the laminate along the x-axis.

For axial Young's modulus of the laminate, we first define the average membrane stresses in the laminate as:

$$\{\bar{\sigma}^m\} = \frac{\{N\}}{z_1 - z_n}. \quad (9)$$

By substitution in Eq. 7, we obtain:

$$\begin{Bmatrix} \bar{\sigma}_{xx}^m \\ \bar{\sigma}_{yy}^m \\ \bar{\tau}_{xy}^m \end{Bmatrix} = \frac{1}{(z_1 - z_n)} \begin{bmatrix} A_{11} & A_{12} & A_{16} \\ A_{21} & A_{22} & A_{26} \\ A_{61} & A_{62} & A_{66} \end{bmatrix} \begin{Bmatrix} \epsilon_{xx}^m \\ \epsilon_{yy}^m \\ \gamma_{xy}^m \end{Bmatrix}, \quad (10)$$

and, by inverting this equation (let $A^* = A^{-1}$) and substituting $A_{12}^* = A_{16}^* = 0$ based on the assumptions above, we infer:

$$\epsilon_{xx}^m = (z_1 - z_n) A_{11}^* \bar{\sigma}_{xx}^m. \quad (11)$$

We therefore define Young's modulus for effective axial elasticity as:

$$E_{xx}^m = \frac{\bar{\sigma}_{xx}^m}{\epsilon_{xx}^m} = \frac{1}{(z_1 - z_k) A_{11}^*}. \quad (12)$$

To find the transverse flexural Young's modulus of the laminate, we first specify the moment-curvature relation of an Euler-Bernoulli beam:

$$M = EI\kappa. \quad (13)$$

Along the x-axis, the second moment of area for a rectangular cross-section is:

$$I_{yy} = \frac{b(z_1 - z_n)^3}{12}. \quad (14)$$

Given the assumption that $M_{yy} = M_{xy} = 0$, the moment along the x-axis is related to the moment of the beam by:

$$M = M_{xx} b. \quad (15)$$

Thus, given the assumption that $D_{12}^* = D_{16}^* = 0$, the Young's modulus for the effective transverse flexural elasticity of the laminate can be found by making Eq. 13 specific to transverse flexure of the x-axis and rearranging the terms:

$$E_{xx}^f = \frac{12M_{xx}}{(z_1 - z_n)^3 \kappa_{xx}}. \quad (16)$$

From inversion of Eq. 7 (let $D^* = D^{-1}$), this reduces to:

$$E_{xx}^f = \frac{12}{(z_1 - z_n)^3 D_{11}^*}. \quad (17)$$

Statistical analysis

Model selection and fitting. In order to explore the relationships between the composite structure and mechanical properties of the cuticle, we fit phylogenetic linear mixed-effects models (PGLMM) to the tensile testing data using maximum likelihood estimation [48–51]. Raw data was processed using a custom script in Python version 3.5.2 [52]. Model exploration and fitting was conducted in R version 3.5.1 (2018-07-02) -- ‘Feather Spray’, using the ‘nlme’ and ‘ape’ packages [53–55]. Response variables and covariates were natural-log transformed, as needed, to ensure that the normalized model residuals were normally distributed [R:shapiro.test] and homoscedastic [R:levene.test], using numerical and graphical analysis (see Supplementary Data). In order to control for phylogenetic non-independence in the data, we included the species of each specimen as a random effect in all models. We also allowed for correlation in the error term of the models, as specified by a variance-covariance matrix generated from a Brownian motion model of trait evolution [R:‘ape’:corBrownian] along a phylogeny [54, 56].

The preferred phylogeny for select North American *Curculio* species is that of Bonal et al. [35]. This phylogeny was generated using Maximum-Likelihood methods; it is untrammatic yet has uniform internal branch lengths. The preferred tree was pruned to include only those species used in tensile testing, with a polytomy at each species' root node to represent the individual specimens examined for that species. Because the branch lengths of the tree were not specified, all branch lengths were set equal to 1.

In general, phylogenetic regression is very robust with respect to missing or incomplete branch length data. Underestimation of branch lengths causes overestimation of phylogenetic signal. This phenomenon was not found to be statistically significant for any of our models. Therefore we consider our study's principal findings to be unaffected by branch length underestimation [56–58].

Other models of trait evolution were considered during model exploration; including Ornstein-Uhlenbeck [R:‘ape’:corMartins] and variable rate (AC/DC) [R:‘ape’:corBlomberg] models [54, 56]. However, neither of these produced a significantly better fit to the data than the Brownian motion model for any comparison, as measured by likelihood score and residual variance; viz. R_σ^2 and $R_{\beta^*}^2$ [R:‘r2glmm’:r2beta] (see Supplementary Data). R_σ^2 is the proportion of generalized variance explained by fixed effects. This measure is generally used for comparison of covariance structures [59–61]. $R_{\beta^*}^2$ measures the multivariate association between the outcome and the fixed effects within a given correlation structure, and is generally used to compare fixed effects [59–61]. Using the R package ‘phytools’ [56, 62], we also estimated the phylogenetic signal in the residual variance of each model; taking into account two measures of spatial autocorrelation (Abouheif's C and Moran's I),

and two measures of phylogenetic signal (Pagel's λ and Blomberg's κ).⁹⁷⁴ section as a fixed effect, with ultimate tensile strength as¹⁰¹⁵
 In all models, we tested whether the inclusion¹⁰¹⁶ the response variable.¹⁰¹⁶

of phylogenetic correlation in the model error produced significantly better model fit, using a likelihood-ratio test [R: 'lmtest': lrtest] and R^2_{σ} -difference test [R: 'r2glmm': r2beta(method='sgv')]⁹⁷⁶ between the strain curve – and the secant modulus at failure. Re-¹⁰¹⁷
 fully-specified model and a model lacking the phylogenetic effect [61, 63]. Models that incorporated covariance due to Brownian motion consistently produced higher likelihood scores and fit to the data. However, no model exhibited statistically significant phylogenetic signal in any of the variables. Once models were fitted to the data, T- and F-statistics were calculated to determine whether each cofactor was significantly different from zero.⁹⁸⁸

Hypothesis testing. Our objectives for hypothesis testing using the PGLMMs were threefold: (1) to assess whether the altered ratio of exocuticle to endocuticle in the rostral apex has an effect on the tensile strength of the rostrum; (2) to test whether a trade-off exists between specimen stiffness and resistance to fracture; and (3) to examine whether rostrum length and flexibility are correlated.⁹⁸⁹

To test the relationship between relative layer thicknesses and tensile strength, we fitted a fully-specified model with the cross-sectional area of exocuticle and endocuticle at the site of fracture as fixed effects, including an interaction term, and with the maximum tensile force sustained prior to fracture as a response variable. This model was then compared to models with only cross-sectional area of either endocuticle or exocuticle, but not both, as the sole fixed effect in the model. We then tested whether one or both regions were significantly correlated to the maximum force sustained in tension, using likelihood-ratio tests and $R^2_{\beta^*}$ -difference tests between each of the three models. Only the cross-sectional area of endocuticle produced a significant fixed effect. We therefore elected to make the model more parsimonious by removing cross-sectional area of exocuticle as a fixed effect. The final model generated for our first aim featured the ratio of exocuticle to endocuticle in cross-

tween specimen stiffness and resistance to fracture. Specimen stiffness was characterized using a low strain elastic modulus – averaged across the first 33% of the stress-strain curve – and the secant modulus at failure. Resistance to fracture was quantified in terms of ultimate strain and fracture toughness, measured as area under the stress-strain curve. Four models were fitted, two of which had ultimate strain as the response variable, and two with fracture toughness as response variable. Each model then used one of the different measures of specimen stiffness as a fixed effect.⁹⁹⁷

Finally, for the third aim we explored whether a size-effect might exist in the *Curculio* rostrum; and specifically if longer and typically more curved rostra were more flexible than shorter, straighter rostra. We generated two models; the low strain and secant elastic moduli individually served as response variables, with specimen length as the fixed effect in both.¹⁰²⁹

Code availability

R, Python, and Matlab scripts used to manipulate and analyze the raw data (as well as their outputs), produce figures, and estimate effective elastic constants are available from the corresponding author upon request.¹⁰³⁷

Data availability

Stress-strain curves for all tensile and fatigue-tested specimens are provided as PDFs (Supplement 1). Diagnostic plots for all PGLMMs are provided as PDFs (Supplement 2). PGLMM terms and output are provided in a PDF (Supplement 3). Raw and processed data will be provided by the corresponding author upon reasonable request.¹⁰⁴¹

1049

REFERENCES

- 1050 [46] Arnett Jr., R. H., Samuelson, G. A., and Nishida G. M. *The Insect and Spider Collections of the World, 2nd Edition*. Fauna and Flora Handbook No. 11. (Sandhill Crane Press, Gainesville, 1993).¹⁰⁵¹
- 1051 [47] The MathWorks, Inc., *MATLAB and Statistics Toolbox* (Natick, Mass., Release R2018b, 2018).¹⁰⁵²
- 1052 [48] Galecki, A. and Burzykowski, T. *Linear Mixed-Effects Models Using R. A Step-by-Step Approach* (Springer, New York, 2013).¹⁰⁵³
- 1053 [49] Hadfield, J. D. and Nakagawa, S. General quantitative genetic methods for comparative biology: phylogenies, taxonomies and multi-trait models for continuous and categorical characters *J. Evol. Biol.* **23:3**, 494–508, (2010).¹⁰⁵⁴
- 1054 [50] Housworth, E. A., Martins, E. P., and Lynch, M. The Phylogenetic Mixed Model *Am. Nat.* **163:1**, 84–96, (2004).¹⁰⁵⁵
- 1055 [51] Stone, G. N., Sean, N., and Felsenstein, J. Controlling for non-independence in comparative analysis of patterns across populations within species *Philos. Trans. Royal Soc. B* **366:1569**, 1410–1424, (2011).¹⁰⁵⁶
- 1056 [52] Python Core Team. *Python: A dynamic, open source programming language* (Python Software Foundation, Version 3.5.2, 2018).¹⁰⁵⁷
- 1057 [53] R Development Core Team *R: A Language and Environment for Statistical Computing* (R Foundation for Statistical Computing, Vienna, Version 3.5.1, 2008).¹⁰⁵⁸

- 1077 [54] Paradis, E. and Schliep, K. ape 5.0: an environment
1078 for modern phylogenetics and evolutionary analyses in
1079 R *Bioinformatics* **5.0**, (2018).
- 1080 [55] Pinheiro, J. et al. nlme: Linear and Nonlinear Mixed
1081 Effects Models **R package version 3.1-137**, (2018).
- 1082 [56] Münkemüller, T. et al. How to measure and test phylo-
1083 genetic signal *Methods Ecol. Evol.* **3:4**, 743–756, (2012).
- 1084 [57] Stone, E. A. Why the phylogenetic regression appears
1085 robust to tree misspecification *Syst. Biol.* **60:3**, 245–260,
1086 (2011).
- 1087 [58] Molina-Venegas, R. and Rodríguez, M. Á. Revisiting
1088 phylogenetic signal; strong or negligible impacts of poly-
1089 tomies and branch length information? *BMC Evol. Biol.*
1090 **17:1**, 1–53, (2017).
- 1091 [59] Nakagawa, S. and Schielzeth, H. A general and simple
1092 method for obtaining R2 from generalized linear mixed-
1093 effects models *Methods Ecol. Evol.* **4:2**, 133–142, (2013).
- 1094 [60] Jaeger, B. C., Edwards, L. J., Das, K., and Sen, P. K.
1095 An R² statistic for fixed effects in the generalized linear
1096 mixed model *J. Appl. Stat.* **44:6**, 1086–1105, (2016).
- 1097 [61] Jaeger, B. Computes R Squared for Mixed (Multilevel)
1098 Models **Version 0.1.2** (2017).
- 1099 [62] Liam, J. R. phytools: An R package for phylogenetic
1100 comparative biology (and other things) *Methods Ecol.
and Evol.* **3**, 217–223, (2012).
- 1101 [63] Zeileis, A. and Hothorn, T. Diagnostic Checking in Re-
1102 gression Relationships *R News* **2:3**, 7–10, (2002).